# Lunar Microwave Brightness Temperature: Model Interpretation and Inversion of Spaceborne Multifrequency Observations by a Neural Network Approach

Mario Montopoli, Alessandro Di Carlofelice, Marco Cicchinelli, Piero Tognolatti, *Member, IEEE*, and Frank S. Marzano, *Senior Member, IEEE*

***Abstract*—Understanding the lunar physical properties has been attracting the interest of scientists for many years. This paper is devoted to a numerical study on the capability of retrieving the thickness of the first layer of regolith as well as the temperature profile behavior from satellite-based multifrequency radiometers at frequencies ranging from 1 to 24 GHz. To this purpose, a forward thermal–electromagnetic numerical model, able to simulate the response of the lunar material in terms of upward brightness temperature ($TB$), has been used. The input parameters of the forward model have been set after a detailed investigation of the scientific literature and available measurements. Different choices of input parameters are possible, and their selection is carefully discussed. By exploiting a Monte Carlo approach to generate a synthetic data set of forward-model simulations, a physically based inversion methodology has been developed using a neural network technique. The latter has been designed to perform, from multifrequency $TB$'s, the temperature estimation at the lunar surface, the discrimination of the subsurface material type, and the estimate of the near-surface regolith thickness. Results indicate that, within the simplified scenarios obtained by interposing strata of rock, ice, and regolith, the probability of detection of the presence of discontinuities beneath the lunar crust is on the order of 84%. The estimation uncertainty of the near-surface regolith thickness estimation ranges from 11 to 81 cm, whereas for the surface temperature, its estimation uncertainty ranges from about 1.5 K to 3 K, conditioned to the choice of radiometric frequencies and noise levels.**

Manuscript received July 1, 2010; revised January 28, 2011; accepted June 11, 2011. Date of publication August 1, 2011; date of current version August 26, 2011. This work was supported in part by the Italian Ministry of University and Research.

M. Montopoli is with the Department of Electrical Engineering and Information, University of L'Aquila, 67100 L'Aquila, Italy, and also with the Center of Excellence for the integration of remote sensing TEchniques and numerical Modelling for the Prediction of Severe weather, University of L'Aquila, 67100 L'Aquila, Italy (e-mail: mario.montopoli@univaq.it).

A. Di Carlofelice and P. Tognolatti are with the Department of Electrical Engineering and Information, University of L'Aquila, 67100 L'Aquila, Italy (e-mail: alessandro.dicarlofelice@univaq.it; franz.cicchinelli@virgilio.it; piero.tognolatti@univaq.it).

M. Cicchinelli is with the Navigation Systems and Services engineering unit, Telespazio S.p.A. (a Finmeccanica/Thales company), 00156 Rome, Italy (e-mail: franz.cicchinelli@virgilio.it).

F. S. Marzano is with the Department of Electronic Engineering, Sapienza University of Rome, 00184 Rome, Italy, and also with the Center of Excellence for the integration of remote sensing TEchniques and numerical Modelling for the Prediction of Severe weather, University of L'Aquila, 67100 L'Aquila, Italy (e-mail: mario.montopoli@univaq.it).

Color versions of one or more of the figures in this paper are available online at http://ieeexplore.ieee.org.

Digital Object Identifier 10.1109/TGRS.2011.2160351

***Index Terms*—Inverse problem, microwave radiometry, Moon exploration, Moon microwave emission, neural network (NN), radiative transfer (RT) model.**

## I. Introduction

In recent years, a relevant number of space missions have been devoted to the study of the Moon. This renewed interest for Moon explorations is motivated by several aspects: 1) the need to find new extraterrestrial resources for sustaining the human activity on the Earth and 2) the opportunity to exploit the Moon as a springboard toward deep space explorations (i.e., toward Mars) [1]. Even though many governments have been reducing funds to their space agencies, some relevant lunar mission has been launched and successfully ended.

Among others, the following missions are worth mentioning: 1) the Lunar Crater Observation and Sensing Satellite [4], aimed at confirming the presence or absence of water ice in a permanently shadowed crater at the Moon's South Pole by observing the plume of debris caused by the impact of a space module on the lunar surface; 2) the Lunar Reconnaissance Orbiter [3], devoted to find safe landing sites, to locate potential resources, to characterize the radiation environment, and to demonstrate new technology such as infrared radiometry and S-band mini synthetic aperture radar; and 3) the Chang E-1 mission [9], [14] which, for the first time, observed the Moon by means of a microwave radiometer. Within this context, in 2006, the European Space Agency approved the feasibility study of the European Student Moon Orbiter (ESMO) mission [17]. In order to accomplish the ESMO mission objectives, a MicroWave Radiometric Sounder (MiWaRS) was selected as a possible payload for flying on board of the ESMO satellite. At the current stage, the ESMO mission is dealing with its so-called phase B.

The appealing feature of the satellite microwave radiometric observation of the Moon is its capability to sound surface and subsurface thermal structure and, to some extent, morphology [6], [10], [12]. A physically based retrieval approach requires a forward model to simulate the microwave radiometer response from space. Several approaches have been proposed and adopted so far with a variable degree of complexity [6], [12]. Within the ESMO MiWaRS feasibility study, a detailed forward numerical model has been developed. This radiative transfer

(RT) model couples a thermal and an electromagnetic (EM) module to simulate the MiWaRS observed brightness temperatures ($TB$'s) due to a thermally and dielectrically stratified lunar medium [2], [5], [13].

The estimation of the lunar regolith thickness by using satellite microwave radiometers is of uppermost interest [1]. Recent results about regolith thickness inversion evidence a good agreement with expected values [9]. The accuracy and the reliability of these results depend both on the choice of the input parameters of the Moon emission forward model and on the accuracy and flexibility associated to the measuring instrument. Despite the recent efforts in the lunar surface and subsurface temperature retrievals by lunar satellite microwave radiometry [21], [22], an effective algorithm capable to discriminate among various subsurface patterns is still an open issue. Indeed, the microwave radiometric estimation of the surface temperature is characterized by a relatively large spatial footprint if compared with similar instrument operating at infrared, but its knowledge supports the accurate retrieval of other lunar parameters.

This paper is devoted to a numerical study on the inverse problem, dealing with the retrieval of subsurface features of the Moon stratigraphy from satellite-based measurements of $TB$'s which would be observed by multifrequency radiometers such as MiWaRS. To this aim, a Monte Carlo simulation data set of $TB$'s for different stratigraphy scenarios has been set up using the microwave radiometric multilayer forward model, previously developed in [2]. Several possible MiWaRS inverse products have been examined together with their expected accuracy: 1) the detection of discontinuities beneath the lunar crust; 2) the estimation of the thickness of the regolith layer; and 3) the estimation of the lunar near-surface temperature [7], [9], [22]. Since the inversion algorithms exploit the *a priori* knowledge of a forward model, the accuracy of MiWaRS products is highly dependent on the modeling choices about the physical and electrical properties of the lunar material. This is a crucial aspect which is thoroughly discussed in this paper through comparisons with available measurements from Apollo missions [6].

This paper is organized as follows. Section II introduces the key aspects of the adopted forward RT model with special attention to the choices related to the input physical parameters, needed to characterize the lunar material. Section III describes the inversion model approaches, based on the neural network (NN) tool, used to carry out the retrievals of the Moon characteristics. Section IV shows the results of the performed inversions, whereas in Section IV, conclusions are drawn.

## II. Forward Model

In order to simulate the microwave radiation emitted by the Moon in terms of azimuthally isotropic brightness temperature, $TB$, the RT problem has been solved using an incoherent approach [16].

### A. Description

The lunar subsurface has been assumed to be vertically stratified with a set of 501 plane-parallel homogeneous layers up to 5-m depth with negligible multiple scattering effects. This is a very common simplification, frequently used in past and recent works [9], [10], [21], for simulating Moon scenarios. It is worth to mention that, with respect to past works, where three homogeneous layers of regolith, rock, and substratum are considered, the adopted RT forward model uses a finer discretization allowing us to describe more accurately the variations of temperature and permittivity along the vertical structure of the Moon stratigraphy. Thus, the RT model here uses two distinct schemes: a nonlinear thermal model (TM) and a plane-parallel EM model. The temperature profiles are obtained by solving the nonlinear thermal transfer equation after defining the density, the specific heat, and the thermal conductivity along the vertical profile of the lunar material [4], [5]. The EM solution, on the other hand, is based on an incoherent approach where the interaction between the upwelling and the downwelling radiation contribution from each layer is taken into account for modeling the resulting $TB$ from the upper layer at the surface level [2], [15]. The EM solution is obtained after modeling the complex permittivity ($\varepsilon$) along the vertical profile of the lunar material, and $TB$'s are provided in a closed form after inverting a matrix of coefficients which describe the EM properties of the considered lunar vertical structure. Coupling the EM and TM solutions, the numerical simulation of $TB$'s as a function of time (i.e., for different solar illumination) and lunar material properties can be obtained. Both the TM and EM simulations have been numerically tested against similar models developed by other authors such as those in [6], [7], [11], [15], and [28]. These tests, not shown here for brevity, lead us to believe that the simulations we use fit well the current state of the art of modeling efforts for Moon studies. Further details about the adopted RT forward model can be found in [2].

Concerning the RT assumption that volume scattering and surface roughness effects are negligible, it should be noted that, at S- and L-bands, volume scattering may be ignored, but at higher frequencies, such as at Ka-band and above, volume scattering can play a role depending upon the particle distribution albedo [15], [25], [26]. The substantial scarcity of information about the vertical profile of the subsurface fragment size distribution has led us to neglect the effect of volume scattering [6]. In regions which contain an average concentration of centimeter-sized and larger sized fragments, the latter is expected to be up to 30% of that due to heat flow [25]. Indeed, at higher frequencies, the microwave penetration capability is limited to upper layers, and this tends to limit the effects of our approximation. Finally, the possible roughness of surface and layer interfaces is also neglected even though it could be included as a proper emissivity parameterization representing the surface height standard deviation through a small perturbation approach [16].

### B. Permittivity Constant Models

This section focuses on the choice of the input parameters of the RT forward model, particularly of the EM variables that, as it will be shown later on, strongly affect the final results. The value of complex permittivity constant, i.e., its real part $\varepsilon'(z, f)$ and imaginary part $\varepsilon''(z, f)$, as a function of frequency $f$ and depth $z$, has a significant impact on the penetration capabilities of microwaves so that their characterization is crucial

for MiWaRS applications as well as for any other instrument operating in the similar range of frequencies (1–24 GHz). It is well established in the literature (e.g., [6]) that, for the lunar regolith, $\varepsilon'$ has a power law relation with material density $\rho$ only, being its frequency dependence negligible

$$\varepsilon'_r(z) = 10^{l\cdot\rho(z)}. \tag{1}$$

In (1), $\rho$ is usually expressed in centimeters, and $l$ is a constant in $\mathrm{cm}^3\cdot\mathrm{g}^{-1}$. On the contrary, $\varepsilon''$ shows a dependence with frequency as well [12]. Note that the frequency dependence of $\varepsilon''$ is not always taken into account, particularly in recent works about microwave radiometric studies of the lunar surface. To our knowledge, the following model of $\varepsilon''$, given in [12], is probably the widest known:

$$\varepsilon''_r(f,z) = 6.079\cdot 10^{-5}\cdot\rho(z)\cdot\varepsilon'_r(z)\cdot f^{0.25}. \tag{2}$$

We have recently proposed an alternative model of $\varepsilon''$ [2], based on a nonlinear regression performed using lunar sample from Apollo mission measurements (see [6] for details about lunar samples). Note that measurements of Apollo lunar samples are reported only in the range of frequencies between 0.5 and 10 GHz. The proposed model of $\varepsilon''$ is as follows:

$$\varepsilon''_r(f,z) = \varepsilon'_r(z)\cdot 10^{[a1\cdot f+a2]\cdot\rho(z)+b\cdot p_{ch}-c} \tag{3}$$

where $a_1$, $a_2$, $b$, and $c$ are empirical regression coefficients and $p_{ch}$ is the percentage of the chemical composition (i.e., dioxide of titanium $TiO_2$ and oxide of iron FeO) in lunar material. The details about the parameters in (3) can be found in [2]. To understand how the proposed permittivity models in (2) and (3) differ to each other, a comparison between them is shown in Fig. 1.

This figure shows the ratio $\varepsilon''/\varepsilon'$ (known as loss tangent) as a function of frequency. Values for material density $\rho$, needed in (2) and (3), are obtained from consolidated hyperbolic relation set up after Apollo 15 and 17 missions (see [6, p.493]). Few available experimental values [6] at frequencies of about 0.5 and 10 GHz are also reported for comparison (see black circles in Fig. 1). From Fig. 1, the model, given in (3), seems to perform better than (2), particularly at 10 GHz. At higher frequencies, due to the absence of experimental measurements, the reliability of (3) is not guaranteed as well as that of (2). However, we can interpret large values of loss tangent, provided by (3), as a conservative choice since penetration capabilities tend to reduce as the loss tangent increases. For frequencies between 1 and 4 GHz, the two models are equivalent. It is worth mentioning that, in [9], the loss tangent has been set, independently from frequency, to 0.001 and 0.10 for regolith and rock, respectively, whereas in [2], the model in (3) leads to average values equal to 0.02 and 0.014, respectively. There is an order of magnitude difference between the two choices performed in [2] and [9]. This leads to different penetration depths as well. They are reported to be on the order of 2 m in [2] and 10 m in [9] at 3 GHz. On the basis of the aforementioned discussion, we believe that the conservative choice of (3) should be preferred in order to provide results which represent, in a way, a "worst" case.

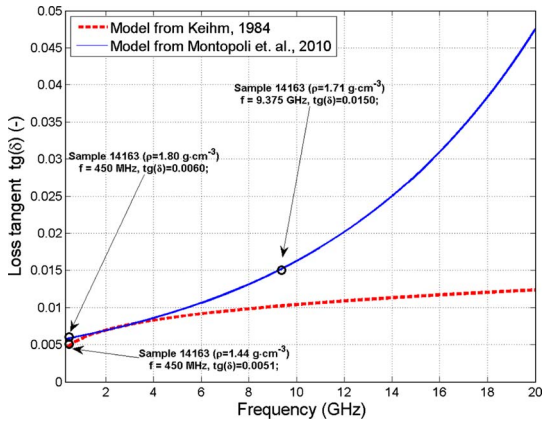


Fig. 1. Loss tangent model behavior. (Blue solid curve) Model from (3). (Red dotted curve) Model from (2). Black circles are measurements on lunar samples listed in [6, Table A9.16].

### C. Forward-Model Setup

Hereinafter, simulations of $TB$'s at frequencies of 1, 3, 12, and 24 GHz have been performed assuming a parameterization scheme as in [2]. Different stratigraphy scenarios have been also simulated. They are composed of stacked slabs of regolith (RS), regolith plus rock (RRS), and regolith, ice, and rock (RIRS) where the letter "$\mathcal{S}$" stands for a scenario. For RRS and RIRS, the thickness of the intermediate slab is varied to include the expected variability of the lunar stratigraphy. The maximum vertical extension of the whole slab is fixed to 5 m. To further describe the uncertainty connected to the knowledge of Moon stratigraphy properties, we have added a random zero mean Gaussian noise to the loss tangent with a 71% of standard deviation with respect to the loss tangent average trend. This choice of the loss tangent variability agrees well with that of measured values listed in [6, Table A9.16].

Two sets of independent synthetic data have been generated for each frequency and Moon "virtual" scenario. The first set is the training data set for training purposes of the inversion algorithms. The second one is the test data set used to calculate the accuracy associated with the microwave radiometric retrievals. A total number of 696 320 samples of $TB$'s have been generated and randomly divided between training and test data sets.

## III. Inversion Model

The goal of the inversion methods, here proposed, is threefold: detect discontinuities beneath the lunar surface and estimate both the thickness of lunar regolith and the surface temperature. To pursue these aims, the forward model, previously described and tuned to simulate $TB$ response from Moon scenarios, has been set up and used to train the proposed inversion algorithms which are principally based on the NN methodology.

### A. NN Retrieval Algorithm

The use of NNs [18] is quite widespread in remote sensing applications [23], [24] even though, to our knowledge, they have never been applied to Moon parameter retrieval purposes.

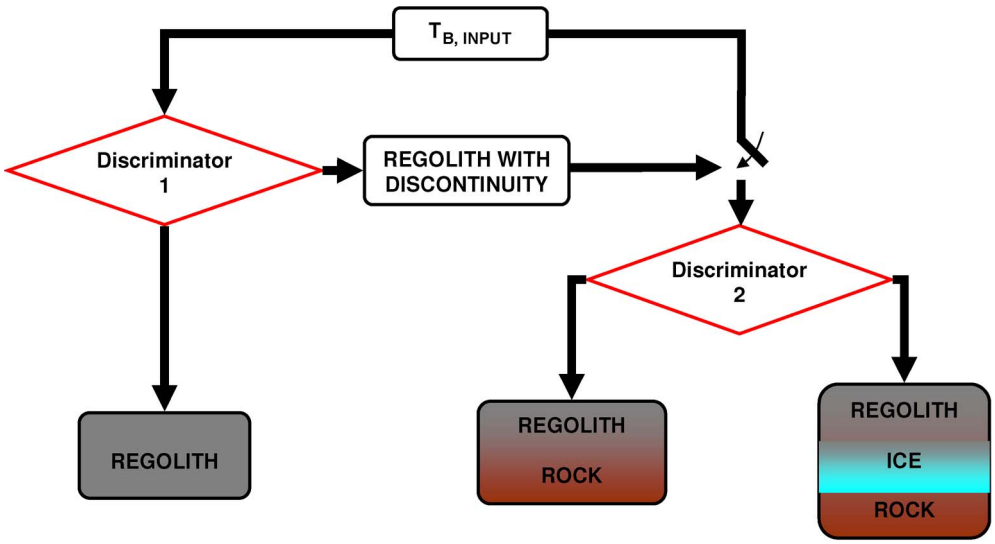


Fig. 2. Schematic flow chart diagram for discontinuity detection algorithm.

An artificial NN is a nonlinear parameterized mapping from an input vector $\mathbf{x}$ to an output $\mathbf{y} = \mathrm{NN}(\mathbf{x}; \mathbf{p}, M)$, where $\mathbf{p}$ is the vector of parameters relating the input $\mathbf{x}$ to the output $\mathbf{y}$, whereas the functional form of the mapping (i.e., the architecture of the net) is denoted as $M$. In our case, the variables $\mathbf{x}$ may represent the multifrequency $TB$'s, whereas $\mathbf{y}$ may be either the surface physical temperature or the soil depth. The multilayer perceptron architecture (MLP), considered here, is a mapping model composed of several layers of parallel processors. It has been theoretically proven that one-hidden-layer MLP networks may represent any nonlinear continuous function [18], while a two-hidden-layer MLP may approximate any function to any degree of nonlinearity taking also into account discontinuities [19]. The architecture $M$ of the NN will be denoted as $M(n_f, h, q)$ for a network with three layers with a number of neurons equal to $h$ and $q$ within each layer, respectively, and where $n_f$ coincides with the number of input variables (i.e., the number of used channel frequencies). The backpropagation training algorithm will be always used to derive the parameters $\mathbf{p}$, if not differently specified. In the following sections, the use of the NN technique for the estimation of the lunar subsurface discontinuity detection, regolith thickness, and surface temperature estimation is described.

*1) Subsurface Discontinuity Detection:* The detection capability of discontinuities beneath the lunar crust, for example, due to the presence of rock or ice within regolith strata, is an important aspect to investigate in order to allow us to identify the regions of the Moon where human outposts are easier to build and human activities will be more sustainable. For this purpose, we have set up a detection scheme, as shown in Fig. 2. Using $TB$'s at all MiWaRS available frequencies, two discrimination algorithms are foreseen. The first one is optimized to distinguish between RS and the other two types of scenarios: RRS and RIRS. The second discriminator is activated on the basis of the output response of the first discriminator, and it substantially tries to distinguish among RRS and RIRS. Both discriminators are based on an NN classifier. After several empirical tests, we found an optimal NN configuration consisting of $M(n_f, 30, 1)$. Note that $n_f$ is left undefined since different choices of input variables are possible. The definition of $n_f$ will be discussed, case by case, in Section IV.

*2) Subsurface Thickness Estimation:* Discontinuities of the material density profiles can be exploited to estimate the regolith (or even ice) thickness. The thickness estimation can be accomplished by detecting the inhomogeneity of the density at the interface between different types of materials. At least two different methods of thickness estimation can be investigated. They are labeled as "direct" and "indirect" methods.

In the "indirect" thickness estimation method, the inspection of the gradients, shown by the vertical profiles of lunar material density, is used to identify their thickness. The "indirect" method requires two steps: the lunar material typology detection (and consequently the definition of a density profile model for each material typology) and the thickness estimation through the gradient analysis of the density profile. On the other hand, the "direct" thickness estimation implies a determination of the position of the discontinuity directly from $TB$'s exploiting the MiWaRS sounding capabilities and the ability of the NN technique to easily describe the functional relation between the multifrequency $TB$'s and the material thickness. Both the "direct" and "indirect" methods have been implemented through an NN, previously set up on a proper training data set.

In order to illustrate the regolith thickness retrieval, Fig. 3 shows an example of density vertical profile for the two cases, namely, RRS and RIRS. Black solid curves represent two input density profiles that we assumed as "truth," whereas red dotted lines are estimates obtained applying the "indirect" method. Due to the high number of sublayers in which the density vertical profiles are discretized, a principal component analysis (PCA) compression has been applied prior to run the NN. The PCA approach, through the computation of the eigenvalues and eigenvectors of the covariance matrix of several density profiles, allows us to define a reduced set of basis vectors that define a new reference system where the density profile vector can be projected. Of course, an inverse PCA transformation

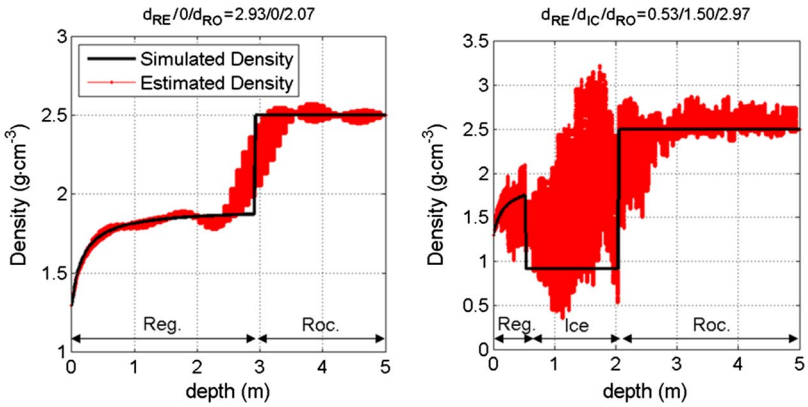


Fig. 3. (Red dotted curves) Examples of density profile estimation for (left panel) (Reg.) regolith and (Roc.) rock scenario and (right panel) regolith, ice, and rock. Black curves refer to the true synthetic profile. Discontinuities of black curves are due to supposed inhomogeneities within lunar scenarios.

has to be applied in order to restore the initial set of bases where the original density profiles were described. The architectures $M(n_f, 10, 40)$ and $M(n_f, 10, 1)$ have been selected for retrieving regolith thickness with "indirect" and "direct" methods, respectively. From Fig. 3, the error variability of the reconstructed density estimates (shown in red colors) is due to the variability we imposed on the loss tangent during the $TB$ simulation. When RRS is considered (left panel), a relatively small error is noticed as opposed to the RIRS case (right panel) where the thickness estimations become very problematic even in the ideal considered case. Of course, it is expected that lunar discontinuities of vertical density profiles are not as sharp as shown in Fig. 3 so that the inversion results have to be regarded as optimistic.

*3) Surface Temperature Estimation:* As a final product of MiWaRS, the surface temperature can be estimated using the higher available frequencies. As mentioned before, MiWaRS is not optimized to provide estimates of surface temperature since its large footprint (approximately between 60 and 90 km at 200-km orbit perigee) can provide only average values on large areas. The selected microwave frequencies (1, 3, 12, and 24 GHz) have not been chosen to optimally sense the thermal properties at the Moon surface, but they can provide an appealing side application of MiWaRS. Anyway, the quantification of the associated errors can represent a valuable effort to complement the surface thermal retrieval by other satellite sensors (i.e., infrared radiometers). The generated synthetic data set allows us to relate the surface temperature $(Ts)$ to brightness temperatures $TB$'s. This relationship for a time period equal to a synodic period (i.e., a lunar day) is shown in Fig. 4.

$TB$ against $Ts$ signatures appear as a nested ovals since, as the time goes on, the solar illumination varies so that a given value of $Ts$ can be registered both when sun rises and sets. At higher frequencies, there is a higher sensitivity of $TB$ with respect to $Ts$ since the energy contribution mainly comes from the upper strata of the Moon. At lower frequencies, the opposite happens. This justifies the flattened shape of the ovals which are correlated with the frequency. From Fig. 4, it appears quite evident that $TB$'s at 24 and 12 GHz are the most suitable for surface temperature estimation. In this case, a feed-forward NN $M(n_f + 1, 10, 1)$ will be used to estimate $Ts$ from $TB$'s. The time information has been also included within the input of the NN to discriminate between lunar day and night, and this allows improving the error score, as will be shown in the numerical result section.

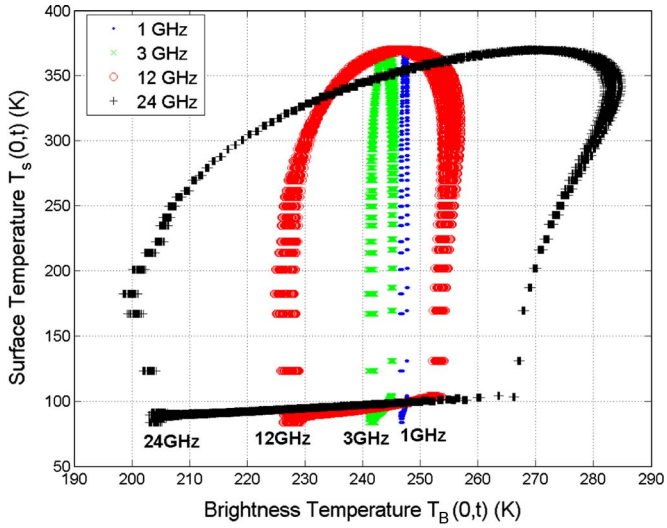


Fig. 4. Simulated brightness temperature at frequencies of (blue, ·) 1 GHz, (green, ×) 3 GHz, (red, ○) 12 GHz, and (black, +) 24 GHz versus surface temperature for a whole lunation period.

## IV. Numerical Results

This section aims at quantifying the inversion results obtained starting from the forward modeling of $TB$'s at 1, 3, 12, and 24 GHz. Inversion algorithms are focused on discontinuity subsurface detection, regolith thickness, and surface temperature estimation.

The following results have been obtained after training the retrieval algorithms, previously described, with a training data set and testing the performance with an independent test data set. The test data set is composed of 87 040 samples. It describes, for each frequency, all scenarios (with RS: 6400 samples; RRS: 32 000 samples; RIRS: 48 640 samples) and the loss tangent variability. The latter has been assumed to be Gaussian distributed with a standard deviation, as described in Section II-C. The large number of simulated samples is due to both the temporal variations and the different thickness configurations

TABLE I
SCORE ERRORS FOR MOON DISCONTINUITY DETECTION PURPOSES WHEN $TB$'S AT 1 AND 3 GHZ ARE USED

| DISCMINATORS | DISCRIMINATOR CHOICES | NOISE FREE $\sigma_n$ = 0 K | | NOISE 1 $\sigma_n$ = 0.5K | | NOISE 2 $\sigma_n$ = 1K | |
|---|---|---|---|---|---|---|---|
| | | POD [%] | FAR [%] | POD [%] | FAR [%] | POD [%] | FAR [%] |
| Discriminator 1 | Only Regolith (RS) or Reg. with discontinuity | 99.42 | 0.71 | 92.71 | 5.39 | 84.58 | 7.49 |
| Discriminator 2 | Reg.,Rock (RRS) or Reg.,Ice,Rock (RIRS) | 72.12 | 26.65 | 70.31 | 30.32 | 70.25 | 30.42 |
| Overall | | 74.80 | 25.20 | 68.86 | 30.66 | 64.92 | 34.84 |

*POD and FAR stand for Probability Of Detection and False Alarm Rate respectively. Reg. stands for Regolith. $\sigma_n$ is the standard deviation of the instrumental noise.*

within a given scenario. Eventually, in order to model the instrumental noise, introduced by the spaceborne radiometer, we have added to the test data set a zero mean white noise with two levels of standard deviation $\sigma_n$ of 0.5 K (noise level 1) and 1 K (noise level 2) as well.

### A. Detecting the Subsurface Discontinuity

After the definition of the test data set, the feed-forward NN, previously introduced, has been trained and applied on it. Different frequency choices for the $TB$ input have been investigated. To select the optimal frequencies among those available for MiWaRS system, the probability of detection (POD) and false alarm rate (FAR) skill scores have been used [20]. POD and FAR are defined as follows:

$$POD = \frac{H}{H+M} \tag{4}$$

$$FAR = \frac{F}{H+F}. \tag{5}$$

In (4) and (5), $H$, $M$, and $F$ stand for hit, misses, and false respectively. $H$ represents the number events where both estimates and the "truth" agree (i.e., when a type of stratigraphy, which really exists in our virtual scenarios, is detected from $TB$'s), $F$ indicates the situations where a type of stratigraphy that does not exist is detected, and $M$ represents the opposite situation where we do not detect a type of stratigraphy that really exists.

On the basis of POD and FAR indexes, we have found that the frequencies of 1 and 3 GHz ($n_f = 2$) provide the best score with respect to other frequency combinations. Table I lists the POD and FAR scores when $TB$'s at 1 and 3 GHz are used to detect discontinuities following the scheme in Fig. 2.

Table I illustrates how the performance of the discriminator 1 in Fig. 2 (i.e., detection of a discontinuity that is the recognition between RS and RRS or between RS and RIRS cases) is different from that of discriminator 2 (i.e., decision about the discontinuity type, that is, between RRS and RIRS once the presence of discontinuity is detected). In our simplified scenarios, the ability of MiWaRS in recognizing the presence of a discontinuity is quite high, from 99% to 84%, depending on the degree of instrumental noise (see Table I, POD score of discriminator 1 where regolith with discontinuity is shown). FAR scores are low as well, and they range from a percentage of 0.71% to 7.49% in the worst case.

After detecting the presence of material discontinuity, the discriminator 2 is applied, but in this case, the POD ranges from 70% to 72% (see Table I, POD score for discriminator 2). In this case, FAR is fairly high with respect to the previous case, and it ranges from about 26% to 30%. These results indicate that the recognition of the type of discontinuity is difficult by MiWaRS, and this is due to the high degree of overlapping among the microwave signatures of the proposed scenarios at the selected frequencies [2]. To have an idea of the whole performance of the detection properties, the overall scores are listed in the last row of Table I as well.

### B. Retrieving Subsurface Thickness

On the basis of the results just shown, it appears reasonable, from MiWaRS, to estimate only the thickness of the regolith. "Direct" and "indirect" methods, discussed in Section III-A2, have been applied on test data set using the frequencies of 1 and 3 GHz. As for the detection problem, other frequency choices tend to lead to worse results. Scatter plots in Fig. 5 show the estimates of the regolith thickness, compared with "true" synthetic values for different scenarios and various degrees of radiometer instrumental error ($\sigma_n = 0$ K, $\sigma_n = 0.5$ K, and $\sigma_n = 1$ K) when the "direct" method is applied. This figure shows both the mutual correlation of the considered variables (i.e., the degree of concentrations of points around the bisector line) and their bidimensional distribution (the color code indicates the density of points in a given portion of the figure). Its analysis indicates that the proposed NN estimator seems to be unbiased in the sense that most of the samples are distributed around the bisector line. By increasing the instrumental noise level, the tails of the distributions increase in size as well, indicating large estimation errors. In order to quantify the performance of thickness estimation, Table II summarizes the estimation errors for both the "direct" and "indirect" methods. The distinction between the retrievals, performed for RRS and RIRS, is also displayed. The "direct" and "indirect" methods perform in a similar way for all noise levels, when RRS is considered. This is due to the fact that, in RRS case, the discontinuities between regolith and rock are sharpened so that they are relatively easy to identify. For a standard deviation instrumental accuracy, $\sigma_n$,

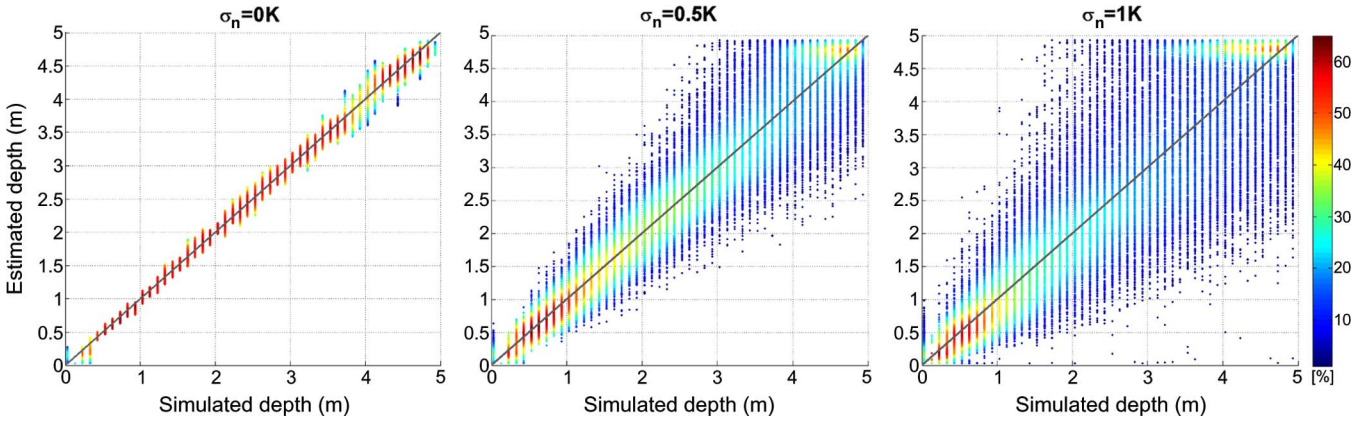


Fig. 5. Scatter plots between simulated "true" and estimated thicknesses for different levels of instrumental noise. (From left to right panels) $\sigma_n = 0$, $\sigma_n = 0.5$ K, and $\sigma_n = 1$ K. Color bar indicates the percentage of samples for each position in the adopted reference system.

TABLE II
REGOLITH THICKNESS ESTIMATION ERRORS USING $TB$'S AT 1 AND 3 GHZ

| | | Rock and Regolith Scenarios | | | Regolith, Rock and Ice Scenario | | |
|---|---|---|---|---|---|---|---|
| ESTIMATIONS METHODS | ERRORS | $\sigma_n = 0$ K | $\sigma_n = 0.5$ K | $\sigma_n = 1$ K | $\sigma_n = 0$ K | $\sigma_n = 0.5$ K | $\sigma_n = 1$ K |
| Direct Thickness Estimation | RMS [cm] | 11.05 | 47.02 | 81.03 | 24.21 | 49.13 | 83.33 |
| | Cc [-] | 0.99 | 0.95 | 0.86 | 0.98 | 0.93 | 0.81 |
| Indirect Thickness Est. | RMS [cm] | 13.99 | 46.95 | 80.12 | 133.30 | 125.50 | 119.40 |
| | Cc [-] | 0.99 | 0.94 | 0.85 | 0.88 | 0.83 | 0.75 |

equal to 1 K, the estimation root mean square error (rmse) is on the order of 80 cm. When the composition of Moon stratigraphy becomes more complex, for example, in the case of RIRS, the errors attributed to the two estimation methods are different. For example, taking the worst case of $\sigma_n$ equal to 1 K, the "direct" method provides an rmse of 80 cm that is sensibly lower than 119 cm which is obtained with the "indirect" method. The correlation coefficients are quite high in all cases (being higher than 0.75).

### C. Surface Temperature

For what concerns the surface temperature $T_s$ retrieval from $TB$'s, the quantitative evaluation of the retrieval errors is listed in Table III. Different choices of the radiometric frequencies are possible: At 24 GHz, with $\sigma_n = 0$ K, we have the best error score (rmse $= 1.44$ K). Similar performances are observed with the choice of the channel at 12 GHz when $\sigma_n = 0.5$ K or $\sigma_n = 1$ K. In summary, the use of 12 or 24 GHz appears to be quite similar for the surface temperature purpose. The joint use of 12 and 24 GHz does not improve the overall estimation temperature scores (for example, when $\sigma_n = 1$ K, we have an rmse $=$ 3.34 K against rmse $= 3.02$ K when 24 GHz is used alone).

The overall results, summarized by Table III, reflect, in some way, the behavior with frequency of $TB$ against $T_s$, shown in Fig. 4, where, as the frequency increases, the relation tends to reduce to a vertical line. Another aspect to observe is that the results listed in Table III are all obtained considering the lunation period as an input variable for the NN-based estimator since this choice allows discriminating between different sun illumination levels. If the lunation period is not considered as an input variable for the surface temperature estimator, the multisolution problem can occur, and worse results are obtained.

TABLE III
SURFACE TEMPERATURE ESTIMATION RMSES

| | INPUT1 | | | INPUT2 | | |
|---|---|---|---|---|---|---|
| | *time* and *freq.*= [12 & 24] | | | *time* and *freq.* = [24] GHz | | |
| | $\sigma_n = 0$ K | $\sigma_n = 0.5$ K | $\sigma_n = 1$ K | $\sigma_n = 0$ K | $\sigma_n = 0.5$ K | $\sigma_n = 1$ K |
| RMSE [K] | 1.54 | 2.14 | 3.34 | 1.44 | 1.85 | 3.02 |
| | INPUT3 | | | INPUT4 | | |
| | *time* and *freq.*= [12] GHz | | | *time* and *freq.* = [3 & 12] GHz | | |
| | $\sigma_n = 0$ K | $\sigma_n = 0.5$ K | $\sigma_n = 1$ K | $\sigma_n = 0$ K | $\sigma_n = 0.5$ K | $\sigma_n = 1$ K |
| RMSE [K] | 1.82 | 2.04 | 2.99 | 2.03 | 2.70 | 5.22 |

## V. CONCLUSION

A numerical evaluation of inversion approaches, capable to retrieve Moon subsurface features from satellite-based brightness temperature at frequencies in the range of 1–24 GHz, has been carried out. The NN methodology has been employed due to its flexibility, easy of use, and accuracy of the estimation results. NNs are trained to pursue three main objectives: the discrimination of the type of material present beneath the lunar surface, the temperature estimation at the lunar surface, and the estimate of the regolith thickness.

Based on forward modeling of Moon response, in terms of brightness temperature, the results indicate how a passive microwave radiometer operating at 1 and 3 GHz with accuracy less or equal to 1 K is able to detect the presence of discontinuities with a POD above 84%. This value is also conditioned to the ideal virtual scenarios we have supposed to simulate and the antenna footprint characteristics. For what concerns the regolith thickness estimation, the expected error score in terms of rmse is on the order of 83 cm with an increasing error as the discontinuity beneath the lunar surface moves toward higher

depths. If a channel at 24 GHz is added to the basic configuration of 1 and 3 GHz, the temperature at lunar surface can be retrieved with an error accuracy of about 3 K. Alternatively, the 12-GHz channel can be used as an alternative to 24 GHz, still maintaining approximately the same degree of accuracy. Another important aspect, discussed in this paper, has been the sensitivity of the final results to the choice of the forward-model input parameters. The choice of material permittivity constants, within the range of possibilities existing in the literature, may strongly influence the final results. Values of loss tangent, in agreement with those collected after the Apollo missions, have been used. These values are generally higher, particularly around the frequency of 10 GHz, with respect to those used in past work. As a consequence, smaller penetrations into lunar material are obtained from our numerical simulations when compared to those available in the literature.

Future works can be devoted to increase the complexity of the proposed scenarios in terms of more accurate EM models and to the application of the proposed inversion methodology to spaceborne microwave radiometric measurements of the Moon surface and subsurface.

## ACKNOWLEDGMENT

The authors would like to thank Dr. R. Walker, Project Manager for Educational Satellite Projects at European Space Agency, and his staff for the opportunity given to design a microwave radiometer for the Moon exploration. The authors would also like to thank all students of the University of L'Aquila and the Sapienza University of Rome for their support.

## REFERENCES

[1] "The scientific context for exploration of the Moon: Final report," Nat. Res. Council Nat. Acad., Washington, DC, 2007, 120 pages.

[2] M. Montopoli, A. Di Carlofelice, P. Tognolatti, and F. S. Marzano, "Remote sensing of the Moon's sub-surface with multi-frequency microwave radiometers: A numerical study," *Radio Sci.*, vol. 46, p. RS1 012, 2011.

[3] M. B. Houghton, C. R. Tooley, and R. S. Saylor, Mission Design and Operational Considerations for NASA's Lunar Reconnaissance Orbiter, IAC-07-C1.7.06.

[4] A. Colaprete, G. Briggs, K. Ennico, J. L. Heldman, L. S. Sollitt, E. Asphaug, D. G. Korycansky, P. H. Schultz, A. Christensen, and K. Galal, "An overview of the lunar crater observation and sensing satellite (LCROSS) mission—A mission to investigate lunar polar hydrogen," in *Proc. 39th Lunar Planet. Sci. Conf.*, Mar. 2008, p. 1838, Contribution No. 1391.

[5] A. Di Carlofelice and P. Tognolatti, "A non-linear circuit model for dynamic evaluation of microwave brightness temperature of the Moon," in *Proc. Eur. Microw. Week*, Rome, Italy, Sep. 28–Oct., 2 2009, pp. 978–981.

[6] G. H. Heiken, D. T. Vaniman, and B. M. French, Eds., *Lunar Sourcebook A User's Guide to the Moon*. Cambridge, U.K.: Cambridge Univ. Press, 1991, p. 736.

[7] J. C. Jaeger, "The surface temperature of the Moon," CSIRO Australia, Provided by the NASA Astrophysics Data System1952.

[8] W. Ji, L. Dihui, Z. Xiaohui, J. Jingshan, A. T. Altyntsev, and B. I. Lubyshev, "Microwave brightness temperature imaging and dielectric properties of lunar soil," *J. Earth Syst. Sci.*, vol. 114, no. 6, pp. 627–632, Dec. 2005.

[9] Y. Q. Jin and W. Fa, "An inversion approach for lunar regolith layer thickness using optical albedo data and microwave emission simulation," *Acta Astronaut.*, vol. 65, no. 9/10, pp. 1409–1423, Nov./Dec. 2009.

[10] S. J. Keihm and M. G. Langseth, "Lunar microwave brightness temperature observations reevaluated in the light of Apollo program findings," *Icarus*, vol. 24, no. 2, pp. 211–230, Feb. 1975.

[11] S. J. Keihm and J. A. Cutts, "Vertical structure effects on planetary microwave brightness temperature measurements: Applications to the lunar regolith," *Icarus*, vol. 48, no. 2, pp. 201–229, Nov. 1981.

[12] S. J. Keihm, "Interpretation of the lunar microwave brightness temperature spectrum: Feasibility of orbital heat flow mapping," *Icarus*, vol. 60, no. 3, pp. 568–589, Dec. 1984.

[13] M. Montopoli, F. S. Marzano, P. Tognolatti, M. Pierdicca, and G. Perrotta, "Remote sensing of the Moon sub-surface from a spaceborne microwawe radiometer aboard the European Student Moon Orbiter (ESMO)," in *Proc. IGARSS*, Barcelona, Spain, 2007, pp. 4451–4454.

[14] H. X. Sun and S. W. Dai, "Mission objectives and payloads for the first lunar exploration of China," in *Proc. 55th Int. Astronautical Congr.*, Vancouver, BC, Canada, 2004.

[15] L. Tsang, J. A. Kong, and K. H. Ding, *Scattering of Electromagnetic Waves*. New York: Wiley, 1985, pp. 200–202.

[16] F. T. Ulaby, R. K. Moore, and A. K. Fung, *Microwave Remote Sensing: Active and Passive*. Reading: Addison-Wesley, 1982, pp. 137–426.

[17] R. Walker and M. Cross, "The European Student Moon Orbiter (ESMO) project attracting and training a new generation of Lunar explorers," *Acta Astronaut.*, vol. 66, pp. 1177–1188, 2010.

[18] S. Haykin, *Neural Networks: A Comprehensive Foundation*. New York: Macmillan, 1995.

[19] E. Sontag, "Feedback stabilization using two-hidden-layer nets," *IEEE Trans. Neural Netw.*, vol. 3, no. 6, pp. 981–990, Nov. 1992.

[20] B. Efron and R. Tibshirani, "Bootstrap methods for standard errors, confidence intervals, and other measures of statistical accuracy," *Stat. Sci.*, vol. 1, no. 1, pp. 54–75, Feb. 1986.

[21] W. Fa and Y.-Q. Jin, "Simulation of brightness temperature from lunar surface and inversion of regolith layer thickness," *J. Geophys. Res.*, vol. 112, p. E05 003, 2007, doi:10.1029/2006JE002751.

[22] W. Fa and Y.-Q. Jin, "A primary analysis of microwave brightness temperature of lunar surface from Chang-E 1 multi-channel radiometer observation and inversion of regolith layer thickness," *Icarus*, vol. 207, no. 2, pp. 605–615, Jun. 2010.

[23] F. Del Frate and G. Schiavon, "Nonlinear principal component analysis for the radiometric inversion of atmospheric profiles by using neural networks," *IEEE Trans. Geosci. Remote Sens.*, vol. 37, no. 5, pp. 2335–2342, Sep. 1999.

[24] L. Tsang, Z. Chen, S. Oh, R. J. Marks, II, and A. T. C. Chang, "Inversion of snow parameters from passive microwave remote sensing measurements by a neural network trained with a multiple scattering model," *IEEE Trans. Geosci. Remote Sens.*, vol. 30, no. 5, pp. 1015–1024, Sep. 1992.

[25] S. J. Keihm, "Effects of subsurface volume scattering on the lunar microwave brightness temperature," *Icarus*, vol. 52, no. 3, pp. 570–584, Dec. 1982, doi:10.1016/0019-1035(82)90017-3.

[26] F. S. Marzano, "Modeling antenna noise temperature due to rain clouds at microwave and millimeter wave frequencies," *IEEE Trans. Antennas Propag.*, vol. 54, no. 4, pp. 1305–1317, Apr. 2006, doi:10.1109/TAP.2005.872571.

[27] B. A. Campbell, D. B. Campbell, J. L. Margot, R. R. Ghent, M. Nolan, J. Chandler, L. M. Carter, and N. J. S. Stacy, "Focused 70-cm wavelength radar mapping of the Moon," *IEEE Trans. Geosci. Remote Sens.*, vol. 45, no. 12, pp. 4032–4042, Dec. 2007.

[28] A. Di Carlofelice, M. Montopoli, P. Tognolatti, and F. S. Marzano, "Moon's sub-surface numerical investigation with multi-frequency microwave radiometers," in *Proc. Rinem*, Benevento, Italy, Sep. 6–10, 2010.

**Mario Montopoli** received the Laurea degree in electronic engineering from the University of L'Aquila, L'Aquila, Italy, in 2004, and the Ph.D. degree in radar meteorology in a joint program between the University of Basilicata, Potenza, Italy, and the Sapienza University of Rome, Rome, Italy.

In 2005, he was with the Centro di Eccellenza per l'integrazione di Tecniche di Telerilevamento e Modellistica Numerica per la Previsione di Eventi Meteorologici Severi as a Research Scientist working on ground-based radar meteorology with a special focus on C-band applications and processing techniques. Since 2006, he has been with the Department of Electrical Engineering and Information, University of L'Aquila, as a Research Assistant.

Dr. Montopoli was a recipient of the Best Paper Award in the European RADar conference held in Sibiu, Romania, in 2010.

**Alessandro Di Carlofelice** received the Laurea degree in electronic engineering from the University of L'Aquila, Italy, in 2006, and the Ph.D. degree in microwave radiometry for remote sensing and biomedical applications in 2011 from the same university.

In July 2006, he joined the European Student Moon Orbiter program supported by the European Space Agency to design a microwave radiometer payload. Since November 2006, he has been with the Exobiology on Mars (EXOMARS) program with Telespazio S.p.A., and his specific task is the detailed analysis and tradeoff of the different communication scenario options for the Rover Operation Control Center in the support of the rover mission operations. From May 2007 to September 2007, he made a grant with the University of L'Aquila by title "Antennas for the air traffic control." For three months (September 2007–December 2007), he joined the testing of hybrid subsystems (transmitter in Ku-band) with Thales Alenia Space S.p.A. Since January 2008, he has been the Coordinator of this project for the microwave radiometer. From December 2008 to June 2009, he joined the design of ultra-wideband (UWB) dipole antenna for military application with Thales Italia S.p.A. Since February 2011, he has been with the Department of Electrical Engineering and Information, University of L'Aquila, as a Postdoctorate Researcher. His research activity is in space systems for telecommunications and remote sensing.

**Marco Cicchinelli** received the Laurea degree (*cum laude*) in telecommunications engineering from the University of L'Aquila, L'Aquila, Italy, in 2010, and the II level postgraduate master in "space and communication systems" promoted by the Space Academy Foundation, Rome, Italy, in 2011.

Since February 2011, he has been with the "Navigation Systems and Services" engineering unit, Telespazio S.p.A. (a Finmeccanica/Thales company), Rome.

**Piero Tognolatti** (M'83) received the Laurea degree (*cum laude*) in electronic engineering from the Sapienza University of Rome, Rome, Italy, in 1981.

From 1982 to 1984, he was with the Research and Development Division, Telespazio S.p.A. From 1984 to 1992, he was a Researcher with the Università degli Studi di Roma "Tor Vergata," Rome, where he was involved with electromagnetic fields. He is currently with the University of L'Aquila, L'Aquila, Italy, where he was an Associate Professor in 1992, a Full Professor of microwaves in 2002, and the Director of the Electrical and Information Engineering Department in 2007. His main scientific activities are the medical applications of electromagnetic fields, microwave radiometry for noninvasive measurement of human body temperature (dealing with both inverse problems and radiometer design), numerical analysis of field problems, film bulk acoustic resonator (FBAR) filters, ultra-wideband (UWB) antennas, and electromagnetic compatibility.

Prof. Tognolatti is a member of the Italian Society of Electromagnetics (SIEm).

**Frank S. Marzano** (S'89–M'99–SM'93) received the Laurea degree (*cum laude*) in electrical engineering and the Ph.D. degree in applied electromagnetics from the Sapienza University of Rome, Rome, Italy, in 1988 and 1993, respectively.

In 1993, he was with the Institute of Atmospheric Physics, National Research Council, Rome. From 1994 to 1996, he was with the Italian Space Agency, Rome, as a Postdoctorate Researcher. In 1997, after being a Lecturer with the University of Perugia, Perugia, Italy, he joined the Department of Electrical Engineering and cofounded the Centro di Eccellenza per l'integrazione di Tecniche di Telerilevamento e Modellistica Numerica per la Previsione di Eventi Meteorologici Severi, University of L'Aquila, L'Aquila, Italy, coordinating the Satellite and Radar Remote Sensing Laboratory. Since 2005, he has been with the Department of Electronic Engineering, Sapienza University of Rome and CETEMPS, where he currently teaches courses on antennas, propagation, and remote sensing. His current research concerns passive and active remote sensing of the atmosphere from ground-based airborne and spaceborne platforms, with a particular focus on precipitation using microwave and infrared data, development of inversion methods, radiative transfer modeling of scattering media, and radar meteorology issues. He is also involved in radio propagation topics in relation to incoherent wave modeling, scintillation prediction, and rain fading analysis along satellite microwave links.

Dr. Marzano was the recipient of the Young Scientist Award of the XXIV Union Radio Scientifique Internationale General Assembly in 1993 and the Alan Berman Research Publications Award from the Naval Research Laboratory, Washington, DC, in 1998. Since 2001, he has been the Italian national delegate for the European Cooperation in the Field of Scientific and Technical Research Actions 720 and 280. Since January 2004, he has been acting as an Associate Editor of the IEEE GEOSICIENCE AND REMOTE SENSING LETTERS.